Effects of Ingredient Proportions on the Performance of α-Cellulose/PLA Mixtures Used for Laser Sintering

Hui Zhang,[a] Yanling Guo,[a,*] David L. Bourell,[b] and Deyu Meng [a]

A new powder feedstock composed of biocompatible and degradable biomass materials was introduced and evaluated for laser sintering in this research. The goal for the material is to facilitate high-value utilization of sustainable materials and expand the variety of feedstock that can be used for laser sintering. It was mechanically mixed with polylactic acid (PLA) powder and the filler of α-cellulose powder in the content of 5 wt%, 10 wt%, 15 wt%, and 20 wt%. The effects of the ingredient proportions were evaluated relative to laser sintering performance of α-cellulose/PLA mixtures. The results revealed that the increasing cellulose loading had almost no influence on the mixtures' glass transition temperature, the melt temperature, and the crystallization temperature; thus, the mixtures would share the same processing parameters with neat PLA during the laser sintering fabrication. Although the cellulose loading reduced the materials' melt fluidity and mechanical properties, it decreased the dimensional deformation of the laser-sintered parts and made the mixture more feasible as the feedstock of laser sintering compared to neat PLA.

Keywords: Laser sintering; α-Cellulose/PLA mixtures; Mass ratio; Thermal properties; Mechanical properties

*Contact information: a: College of Mechanical and Electrical Engineering, Northeast Forestry University, Harbin, Heilongjiang Provence 150040 China; b: Department of Mechanical Engineering, the University of Texas, Austin, Texas 78712 USA; *Corresponding author: nefugyl@nefu.edu.cn*

INTRODUCTION

Laser sintering (LS) is a prevailing additive manufacturing (AM) technology that uses one or more lasers selectively to fuse the powder material layer by layer until finishing the whole part (Bourell 2016). LS technology can cost-effectively manufacture products with sophisticated structure because it produces the parts without supporting structures based on the 'dispersion-deposition' formation method (Schmid *et al.* 2014). Moreover, LS is an attractive pathway for the fabrication of porous parts with tailored properties by either controlling the processing parameters or using designed composites. This method has applications in several industries, including bone tissue engineering scaffolds (Tan *et al.* 2005), implants, and drug delivery with the structure of intricate internal and external geometries (Hollister 2005; Poomathi *et al.* 2019).

Obtaining more sustainable, low-price, and high-performance materials is a core task for the progression of LS technology (Roberts *et al.* 2016; Yu *et al.* 2017). Due to the generally low thermal diffusivity of polymers and relatively low price (Nakano and Ishimoto 2015), polymeric powders used for LS are well accepted compared with metal-based and ceramic-based composites. Among the polymeric feedstocks being used for LS, polylactic acid (PLA), polycaprolactone (PCL) (Williams *et al.* 2005; Lee *et al.* 2013; Doyle *et al.* 2014), polyvinyl alcohol (PVOH) (Chua *et al.* 2004; Shuai *et al.* 2014), poly(3-hydroxybutyrate-co-3hydroxyvalerate; PHBV) (Duan *et al.* 2011; Diermann *et al.* 2019),

and polyether-ether-ketone (PEEK) particles (Tan *et al.* 2003; Schmidt *et al.* 2007) show potential in bioprinting applications due to their biocompatibility (González-Henríquez *et al.* 2019). PLA, PCL, and PHBV have degradability, while PVOH and PEEK are not biodegradable *in vivo*. Nanoparticles and biological ceramics such as hydroxyapatite (HA), calcium silicate ($CaSiO_3$) (Shuai *et al.* 2014), and beta-tricalcium phosphate (β-TCP) (Doyle *et al.* 2014) are added to improve the forming properties, degradability, and biological activity (González-Henríquez *et al.* 2019).

PLA is derived from agricultural sources such as fermented corn. It is an environmentally friendly thermoplastic characterized by compostability, biodegradability, and biocompatibility. In AM technologies, PLA and its composites are widely fabricated as the commercial feedstock of fused deposition modeling (FDM). However, PLA is not commercially available in a powder form with a size below 100 μm, and it is hard to control the thermal deformation of semi-crystalline PLA caused by instantaneous laser energy within an acceptable range. Consequently, only a limited number of studies have dealt with the LS of PLA-based materials.

Cellulose is another biodegradable material from agricultural sources. As an important structural component of the primary cell wall of green plants, cellulose is the most abundant biological macromolecule on earth (Song *et al.* 2015; Yang *et al.* 2015). Additionally, cellulose shows many advantages including its relative low density, high acoustic damping, and low price (Berglund and Peijs 2010). It is widely used as a filler to improve the materials' properties in a variety of applications. However, natural fibers/PLA composites to be used as feedstocks of LS have not been well exploited so far.

This research introduced a new type of biodegradable wood-plastic composite to be used for LS, which consisted of cellulose powder and PLA 3001D, abbreviated CPLA here. Cellulose powder acted as the filler to improve the LS formability of PLA powder, which was also intended to decrease the shrinkage and deformation of the material during the LS processing (Fig. 1). This study investigated the LS fabrication of CPLA mixtures and assessed the effect of the ingredient proportion on the performance of their laser-sintered parts. The thermal behavior and the melt fluidity of neat PLA and CPLA mixtures with different cellulose loadings were measured. Proper processing parameters for laser sintered neat PLA and CPLA mixtures were obtained based on LS tests and the analysis of material thermal properties. The effect of cellulose loading on the mechanical properties and dimensional accuracy was analyzed.

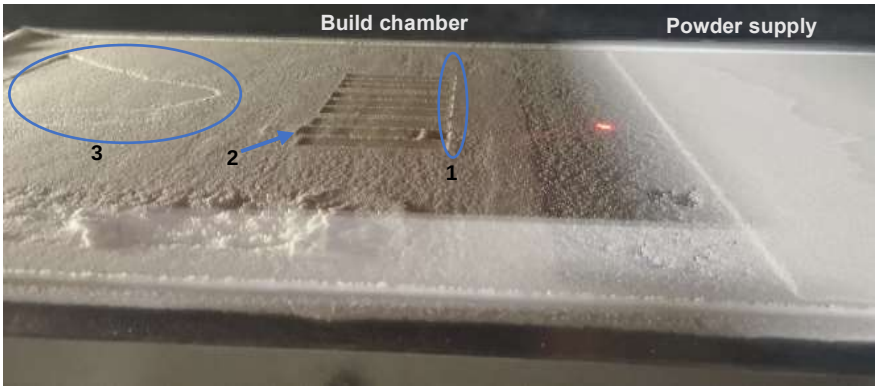

Fig. 1. Laser sintering of neat PLA: (1) Warping near the parts' edge; (2) displacement caused by the deformation; (3) lack of feedstock caused by the shrinkage of PLA

EXPERIMENTAL

Materials Preparation

PLA, $(C_3H_4O_2)_n$, consisting of lactic acid monomer, is produced in bulk by ring-opening polymerization of lactides (Rezgui *et al.* 2005). The PLA used was Ingeo™ 3001D (injection-molding grade), which is supplied in pellet form by NatureWorks LLC (Blair, USA) with the density of 1.24 g/cm^3. PLA 3001D was mostly poly L-lactic acid (PLLA) with a D-lactide content of 1.4% (Tábi *et al.* 2018).

The pellets were crushed cryogenically into white powders by eSUN (Shenzhen, China) with a loose density of 0.62 g/cm^3. However, it is difficult to obtain spherical and subglobose PLA powders by comminution due to its tacky nature (Thittikorn *et al.* 2007). As a result, the microstructure of the PLA particulate was irregular in size and shape. The particle size was approximately 200 μm. Some PLA powders were pulled into long fibers, which led to inferior flowability during the powder spreading processing by the device roller.

The α-cellulose powder, $(C_6H_{10}O_5)_n$, which is composed of parallel homopolymers of (1→4)- β-linked D-glucose monomers (Bučko *et al.* 2011), was purchased from Aladdin Industrial Corporation (Shanghai, China). The fiber size was less than 25 μm, much smaller than the particle diameter of the PLA powder.

Before the preparation of CPLA mixtures, the cellulose fibers and PLA 3001D powders were oven dried at 60 °C for 8 h in an incubator to lower the moisture content and avoid hydrolytic degradation (Tábi *et al.* 2018) during LS processing. The dried cellulose fiber and PLA 3001D powder were put into a high-speed mixer and mechanically mixed below 45 °C in different mass ratios. They were initially mixed for 15 min at a low speed of 750 RPM and then for 5 min at a high speed of 1500 RPM. Finally, different CPLA mixtures with 5 to 20 wt% cellulose loading were prepared.

Laser Sintering Experiments

Laser sintering (LS) experiments were conducted using an AFS-360 rapid prototyping machine (Fig. 2; Longyuan AFS Co., Ltd., Beijing, China) with a build chamber of 360 × 360 × 500 mm^3. The essential parameters of the machine include a CO_2 laser with a wavelength of 10.6 μm, maximum laser power of 55 W, and laser beam diameter of approximately 0.4 mm.

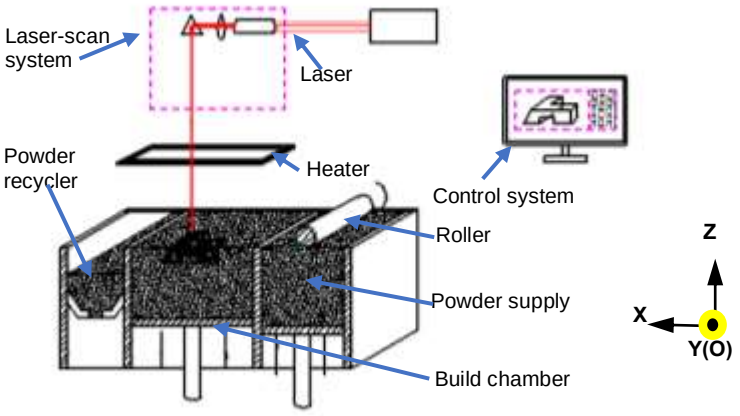

Fig. 2. Schematic of process system of AFS-360 rapid prototyping machine

The LS tests of neat PLA powder were carried out before the CPLA mixture experiments to investigate the feasibility of processing PLA 3001D. Based on thermal properties of materials and 5-layer LS tests of CPLA mixtures, proper process parameters of LS for both PLA 3001D and CPLA composites were established as follows: preheating temperature of 145 °C for 2 h, processing temperature of 135 to 140 °C, laser power of 20 to 24 W, scan speed of 1.6 to 2.2 m/s, scan spacing of 0.1 to 0.2 mm, and layer thickness of 0.25 mm.

Characterization of CPLA Mixtures and Laser-sintered Parts

The thermal behaviors and crystallinity for PLA 3001D powder and CPLA mixtures were evaluated using an STA449F3 simultaneous thermal analyser (STA; Netzsch, Selb, Germany). The 4.8 mg (± 0.2) specimens were scanned at 10 °C/min over the temperature range of 40 to 250 °C. The crystallinity was calculated from the first heating scan according to Eq. 1,

$$X = \frac{\Delta H_m - \Delta H_{cc}}{\Delta H_f} \times 100\%, \Delta H_f = 93 \text{J/g} \quad (1)$$

where X (%) is the calculated crystallinity, ΔH_m (J/g) and ΔH_{cc} (J/g) are the enthalpy of fusion and the enthalpy of cold crystallization, respectively, and ΔH_f (J/g) is the enthalpy of fusion for 100% crystalline PLA.

The SRZ-400E melt flow rate testing equipment (Changchun Intelligent Instrument equipment Co., Ltd., Changchun, China) was used to investigate the flowability of PLA 3001D and CPLA mixtures over the temperature range 170 to 190 °C with a load of 2.16 kg according to ISO1133(2005). Testing materials in the charging barrel were preheated for 10 min before the test began. The results are shown as mean ± SEM (°C/10 min @2.16 kg).

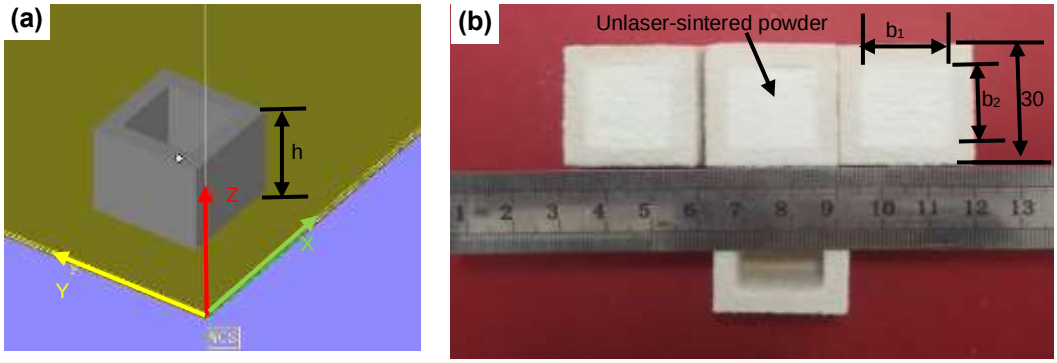

Fig. 3. The laser-sintered cubes for testing the density of powder bed: (a) the 3D model; (b) the laser-sintered cubes

To obtain the density of powder bed of CPLA mixtures with different mass ratio, hollow cubes without lids were fabricated using the responding feedstock *via* LS. The inside stored the unlaser-sintered powders representing a part of the powder bed. The size of the hollow cube (Fig. 3(a)) was 30 × 30 × 30 mm^3, with the wall thickness approximately equal to 5 mm of each side. The density of the powder bed was calculated according to Eq. 2, when the stored powder weight and laser-sintered cube volume ($b_1 \times b_2 \times h$) in Fig. 3(b) were measured. The density of cellulose was measured by the traditional calculation.

$$\rho = \frac{m}{b_1 \times b_2 \times h} \quad (2)$$

Dumbbell-shaped tensile specimens (Fig. 4 (a)) with dimensions of 166 mm × 13 mm × 3.2 mm were fabricated for tensile testing (Fig. 4 (b)). The crosshead speed was 5 mm/min according to ASTM D638-14 (2014). Thin specimens of 127 mm × 12.7 mm × 3.2 mm (Fig. 4 (c)) were tested to obtain flexural strength of laser-sintered parts according to the 3-point bending method (Fig. 4 (d)) of ASTM D790-17 (2017). The support span was 60 mm, crosshead speed was 2 mm/min, and midspan deflection was 15 mm.

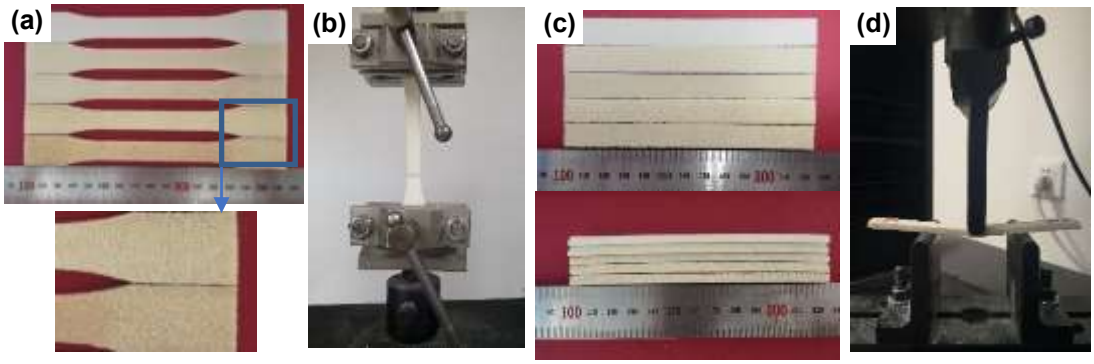

Fig. 4. The mechanical test and the testing specimens: (a) tensile specimens; (b) tensile test; (c) flexural specimens; (d) flexural test

The dimensional relative error value in the X-Y plane and the Z direction of laser-sintered parts was analyzed. The calculation of relative error value was operated in terms of Eq. 3,

$$V_r = \frac{R_{ac} - R_{id}}{R_{id}} \times 100\% \quad (3)$$

where V_r is the dimensional relative error (%), R_{ac} is the present value obtained by measuring the length of the laser-sintered part in the different directions (mm), and R_{id} is the ideal value of the length of the model in the corresponding directions (mm). For the results, '+' means the LS parts get expanded, and '–' means the LS parts are shrunk.

RESULTS AND DISCUSSION

Thermal Properties α-Cellulose/PLA Mixtures

Figure 5 depicts thermal phase transition of PLA 3001D and CPLA mixtures with the cellulose loading content of 5 wt%, 10 wt%, 15 wt%, and 20 wt%. The glass transition temperature (T_g) of PLA 3001D was observed at 61 °C, and its melt temperature (T_m) was 165 °C. PLA 3001D had two crystallization peaks situated at T_{cc1} = 89 °C and T_{cc2} = 151 °C. PLA presents several crystal forms, including α", α', α, β, γ, and ε (Huang *et al.* 2011; Marubayashi *et al.* 2012). The less-ordered α' form crystal is prevalent in PLA 3001D because its crystallization temperature is below 100 °C (Huang *et al.* 2011; Tábi *et al.* 2016). The small exothermal peak was attributed to the disorder-to-order (α'-to-α) phase transition, and thus, the chain packing of the crystal lattice became more compacted (Zhang *et al.* 2008). Comparing these five curves, the increasing cellulose loading had almost no

influence on the T_m, but it decreased the T_g values slightly. The T_g of CPLA declined slightly from 61 °C to 56 °C as the cellulose increased from 0 to 20 wt%, along with a decreasing thermal stability. The T_m reached the top peak from 165 °C to 167 °C when the cellulosed added was 10 wt% and then dropped to 164 °C for 20 wt%-CPLA. Generally, the effect of cellulose loading on the T_m was not obvious and regular, which could be neglected.

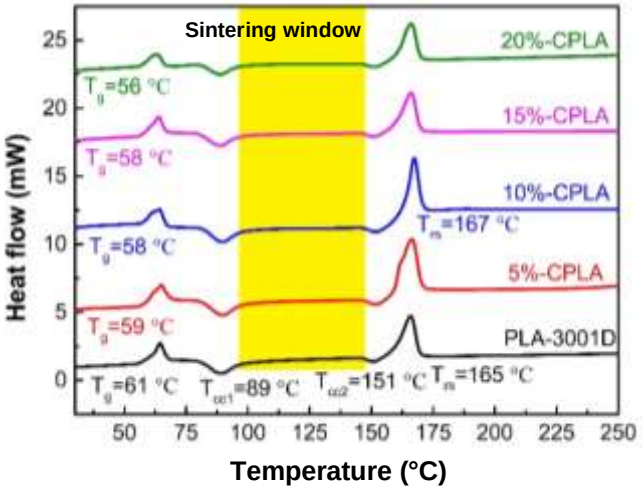

Fig. 5. The thermal behaviors of PLA 3001D and CPLA mixtures

The sintering window in the LS process, representing the range of the proper processing temperature, is usually determined by the feedstock thermal behaviors. For semi-crystalline polymers, the sintering window is located at the interval of between the onset of T_{cc} and the caking temperature (T_a). Therefore, the processing temperature of PLA and CPLA should be above 100 °C (the onset of T_{cc}) and below 156 °C (the onset of T_m). Sequentially, the T_a of 148 °C was acquired *via* the LS testing. The sintering window of PLA and CPLA was finally set as (100 °C, 148 °C). Considering decreasing the laser power and heat accumulation during the preheating and LS processing, the processing temperature was set at (135 °C, 140 °C).

The enthalpy of cold crystallization (ΔH_{cc1}), the enthalpy of fusion (ΔH_m), and the calculated crystallinity (X(%)) are listed in Table 1. The results verified that 5%-CPLA and 10%-CPLA had higher crystallinity but 15%-CPLA and 20%-CPLA had lower crystallinity than neat PLA 3001D. That is to say, the cellulose loading less than 15 wt% might have acted as the nucleating agent to facilitate the crystallization of PLA 3001D .

Table 1. Enthalpy and Crystallinity of PLA and CPLA

Materials	ΔH_{cc1} (J/g)	ΔH_{cc2} (J/g)	ΔH_m (J/g)	X (%)
PLA 3001D	8.60	1.55	19.81	10.39
5%-CPLA	9.45	3.31	27.91	16.29
10%-CPLA	8.98	2.97	22.32	11.15
15%-CPLA	7.78	1.67	18.95	10.21
20%-CPLA	6.12	1.93	16.63	9.22

Melt Fluidity of α-Cellulose/PLA Mixtures

Figure 6 addresses the effects of temperature (170 to 190 °C) and the amount of cellulose loading on the melt flow index (MFI) and the appearance of neat PLA 3001D and CPLA. The melt fluidity of all samples was improved with increased heating temperature. The MFI of PLA 3001D grew slowly over 175 ℃, and thus it was lower than that of all four CPLA mixtures at 190 °C. For CPLA mixtures, the MFI generally decreased with increasing cellulose powder loading from 5 to 20 wt%.

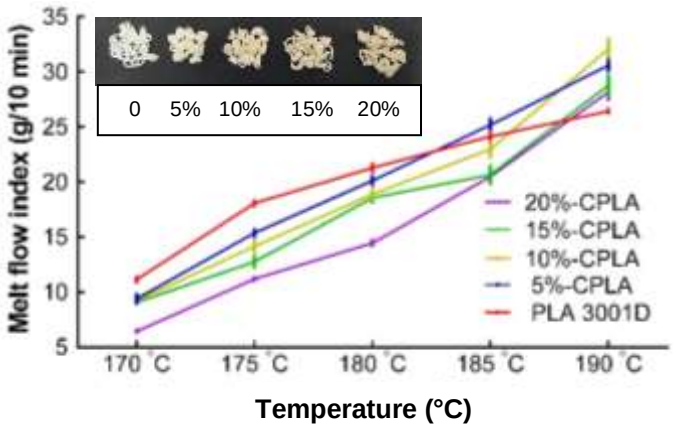

Fig. 6. Melt flow index of PLA 3001D and CPLA mixtures

The melt shear viscosity and component compatibility of materials account for the observed dependence of MFI on temperature and amount of cellulose powder. Within certain conditions, the melt viscosity of polymer-based composites decreases with increasing temperature, leading to better melt flowability and higher MFI (Fujiyama and Kondou 2003; Speranza *et al.* 2014; Mazzanti *et al.* 2016; Cobos *et al.* 2019). In addition, the non-molten cellulose fibers increase the melt viscosity of CPLA, causing a lower MFI with the increasing amount of cellulose fibers (Golzar *et al.* 2012; Harnnarongchai *et al.* 2012; Mazzanti and Mollica 2017; Rokkonen *et al.* 2019). Notably, the MFI of PLA 3001D was lower than that of some CPLA mixtures when the temperature exceeded 183 °C. The reason for this phenomenon might be obtained from the experimental observation that the melt PLA at 190 °C was no longer able to stay in good shape to flow down directly, and some liquid PLA even coagulated near the device's flow channel, leading to declining MFI.

Density of Powder Bed

Table 2 lists the density of neat PLA 3001D, neat cellulose, and CPLA mixtures. The theoretical value of the density powder bed of CPLA mixtures was calculated by Eq. 4, assuming that the space among the PLA particles would not be filled with the smaller cellulose fibers. In Eq. 4, D_{theo} is the theoretical density (g/cm^3), m is the mass content of CPLA powder on the powder bed (g), ρ_p is the density of PLA 3001D powder (g/cm^3), ρ_c is the density of the cellulose powders (g/cm^3), and x is the percentage of content of cellulose (wt%, x=5 wt%, 10 wt%, 15 wt%, 20 wt%).

$$D_{theo} = \frac{m}{v_p + v_c} = \frac{m}{\frac{m \times (100\% - x)}{\rho_p} + \frac{m \times x}{\rho_c}} = \frac{\rho_p \times \rho_c}{\rho_p \times x + \rho_c \times (100\% - x)} = \frac{0.6170.276}{0.617x + 0.276 \times (100\% - x)} \quad (4)$$

The experimental value was obtained in terms of the method mentioned in the section of "Characterization of CPLA Mixtures and Laser-sintered Parts". The filler of cellulose theoretically made the CPLA more lightweight than neat PLA based on the experimental values. Additionally, the density of the CPLA powder bed should decrease theoretically with the increasing cellulose, as shown in Table 2. In fact, the results listed in Table 2 demonstrated that all the experimental values of density for CPLA mixtures were higher than their theoretical value, verifying that the small particles of cellulose would fill the micropores among the big PLA particles and make the CPLA powder bed denser than the theoretical situation. But it was also noticeable that the experimental value declined to the minimum value of 0.563 g/cm^3 when the amount of cellulose loading was 10 wt% and then went up to 0.605 g/cm^3 when the content of cellulose fibers was 20 wt%. Presumably, this tendency is because the effect of lightweight cellulose fiber on decreasing the density of the CPLA mixture played a more important role for CPLA mixtures with the content of cellulose less than 10 wt%, and after that the influence of smaller cellulose fibers on densifying the CPLA mixtures was the dominant factor affecting the experimental density of CPLA mixtures.

Table 2. Density of PLA and CPLA Mixtures

Materials	PLA 3001D	5%-CPLA	10%-CPLA	15%-CPLA	20%-CPLA	Cellulose
Theoretical value (g/cm^3)	0.617	0.583	0.551	0.522	0.497	0.276
Experimental value (g/cm^3)	0.617	0.610	0.563	0.568	0.605	0.276

Mechanical Properties of Laser-sintered α-cellulose/PLA Parts

The tensile strength and flexural strength of laser-sintered parts are depicted by histogram in Fig. 7. They decreased with the increase of cellulose powder loading. When cellulose powder accounted for 15 to 20 wt%, the mechanical strength of laser-sintered CPLA parts dropped dramatically compared with PLA 3001D, and the parts showed poor mechanical properties and were no longer feasible for use.

The mechanical performance of laser-sintered CPLA parts was correlated with the trend observed in the MFI values as a function amount of cellulose fibers. The viscosity of the melt increased with increasing amount of cellulose, and thus the MFI decreased. Moreover, the coalescence and sintering kinetics of the polymers would be retarded, leading to declined bonding degree between the particles. Besides, the mechanical strength of laser-sintered CPLA parts was also related to the degree of the interfacial bonding

between the particles on the micro level. The melt PLA particles during the LS processing acted as the binder to bond with the cellulose fibers or bond with the adjacent particles. The less the binder was, the weaker the interfacial bonding was. As a consequence, the worse the mechanical properties of laser-sintered CPLA parts would have with the increasing cellulose contents.

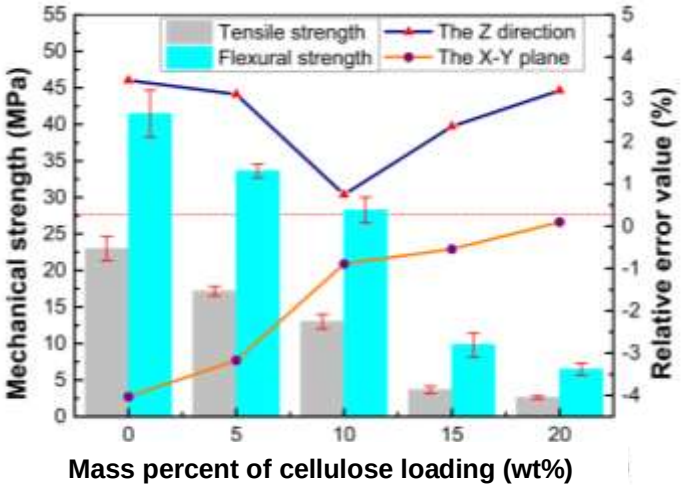

Fig. 7. Mechanical properties and dimensional accuracy of laser-sintered CPLA parts with different contents of cellulose loading

Dimensional Accuracy of Laser-sintered α-cellulose/PLA Parts

As the motion of melt PLA particles was limited due to the resistance from cellulose fibers, the shrinkage and residual stress generated from solidification of melt PLA were reduced with more cellulose powder supporting the part structure. The visible deformation, including the shrinkage and curling of laser-sintered CPLA parts, decreased.

The line graph in Fig. 7 verified that cellulose fiber reduced the shrinkage of the laser-sintered parts. It shows that 20 wt% CPLA had the lowest relative error value in the X-Y plane, and 10% C-PLA had the lowest relative error value in the Z direction fabricated by the AFS-360 rapid prototyping machine (The coordinate system of the parts is consistent with that of the machine shown in Fig. 2). By comparing both the mechanical properties and dimensional accuracy of the laser-sintered CPLA parts, it is thought that 10 %-CPLA is a more promising feedstock for LS and has practical applications due to a combination of higher dimensional accuracy and acceptable mechanical properties.

CONCLUSIONS

1. A new biomass feedstock (CPLA) was manufactured using laser sintering technology, It was composed of the commercial polylactic acid (PLA) powder and the α-cellulose fiber with the advantages of biodegradability, biocompatibility, and environmentally friendly character.
2. A proper range of processing parameters for laser sintering CPLA mixtures was obtained according to the materials' thermal characteristics and LS tests: preheating temperature 145 °C, processing temperature 135 to 140°C, the laser power 20 to 24 W, scan speed 1.6 to 2.2 m/s, scan spacing 0.1 to 0.2 mm, and layer thickness 0.25 mm.

Besides, further study is essential to focus on the parameter optimization in order to get better forming properties of the laser-sintered CPLA parts.

3. The addition of cellulose fiber (≤ 20 wt%) almost had no effect on the thermal properties of the CPLA mixtures, but it reduced the melt flow index of the mixtures. The CPLA mixtures with the 5 wt% or 10 wt% cellulose addition showed higher crystallinity compared with the neat PLA powder.
4. The increasing cellulose loading decreased the deformation of laser-sintered parts caused by the shrinkage and curling of PLA. However, the mechanical properties of the mixtures' laser-sintered parts were weakened as the amount of cellulose fiber increased. Thus, there is a need for a balance between dimensional accuracy and mechanical properties for CPLA mixtures in terms of specific applications.

ACKNOWLEDGMENTS

The authors are grateful for the support of the Natural Science Foundation of Heilongjiang Province (grant number ZD2017009), the National Key R&D Program of China (grant number 2017YFD0601004), the Fundamental Research Funds for the Central Universities (grant number 2572018AB27), and 'Double First-Class' Fund of Northeast Forestry University (grant number 41113253).

REFERENCES CITED

ASTM D638 (2014). "Standard test method for tensile properties of plastics," American Society fir Testing and Material, West Conshohocken, Pennsylvania.

ASTM D790 (2017). "Standard test method for flexural properties of unreinforced and reinforced plastics and electrical insulating materials," American Society fir Testing and Material, West Conshohocken, Pennsylvania.

Berglund, L. A., and Peijs, T. (2010). "Cellulose biocomposites—From bulk Moldings to nanostructured systems," *MRS Bull*. 35(3), 201-207. DOI: 10.1557/mrs2010.652

Bourell, D. L. (2016). "Sintering in laser sintering," *JOM-US* 68(3), 885-889. DOI: 10.1007/s11837-015-1780-2

Bučko, T., Tunega, D., Ángyán, J. G., and Hafner, J. (2011). "*Ab initio* study of structure and interconversion of native cellulose phases," *The Journal of Physical Chemistry A* 115(35), 10097-10105. DOI: 10.1021/jp205827y

Chua, C. K., Leong, K. F., Tan, K. H., Wiria, F. E., and Cheah, C. M. (2004). "Development of tissue scaffolds using selective laser sintering of polyvinyl alcohol/hydroxyapatite biocomposite for craniofacial and joint defects," *J. Mater. Sci. Mater. Med.* 15(10), 1113-1121. DOI: 10.1023/B: JMSM.0000046393.81449.a5

Cobos, C. M., Garzón, L., López Martinez, J., Fenollar, O., and Ferrandiz, S. (2019). "Study of thermal and rheological properties of PLA loaded with carbon and halloysite nanotubes for additive manufacturing," *Rapid Prototyping J.* 25(4), 738-743. DOI: 10.1108/RPJ-11-2018-0289

Diermann, S. H., Lu, M., Dargusch, M., Grøndahl, L., and Huang, H. (2019). "Akermanite reinforced PHBV scaffolds manufactured using selective laser sintering," *J. Biomed. Mater. Res. Part B* 00B, 1-15. DOI: 10.1002/jbm.b.34349

Doyle, H., Lohfeld, S., and McHugh, P. (2014). "Predicting the elastic properties of selective laser sintered PCL/β-TCP bone scaffold materials using computational Modelling," *Ann. Biomed. Eng.* 42(3), 661-677. DOI: 10.1007/s10439-013-0913-4

Duan, B., Cheung, W. L., and Wang, M. (2011). "Optimized fabrication of Ca-P/PHBV nanocomposite scaffolds via selective laser sintering for bone tissue engineering," *Biofabrication* 3(1), 015001. DOI: 10.1088/1758-5082/3/1/015001

Fujiyama, M., and Kondou, M. (2003). "Effect of gelation on the flow processability of poly(vinyl chloride)," *J. Appl. Polym. Sci.* 90(7), 1808-1824. DOI: 10.1002/app.12817

Golzar, M., Jam, N. J., and Behravesh, A. H. (2012). "Mathematical and experimental study on flow of wood plastic composite to acquire its constitutive equation," *J. Reinf. Plast. Comp.* 31(11), 749-757. DOI: 10.1177/0731684412444911

González-Henríquez, C. M., Sarabia-Vallejos, M. A., and Rodriguez-Hernandez, J. (2019). "Polymers for additive manufacturing and 4D-printing: Materials, methodologies, and biomedical applications," *Prog. Polym. Sci.* 94, 57-116. DOI: 10.1016/j.progpolymsci.2019.03.001

Harnnarongchai, W., Kaschta, J., Schubert, D. W., and Sombatsompop, N. (2012). "Shear and elongational flow properties of peroxide-modified wood/low-density polyethylene composite melts," *Polym. Composite.* 33(11), 2084-2094. DOI: 10.1002/pc.22351

Hollister, S. J. (2005). "Porous scaffold design for tissue engineering," *Nat. Mater.* 4(7), 518-524. DOI: 10.1038/nmat1421

Huang, S., Li, H., Jiang, S., Chen, X., and An, L. (2011). "Crystal structure and morphology influenced by shear effect of poly(l-lactide) and its melting behavior revealed by WAXD, DSC and *in situ* POM," *Polymer* 52(15), 3478-3487. DOI: 10.1016/j.polymer.2011.05.044

ISO 1133 (2005). "Plastics-Determination of the melt mass-flow rate (MFR) and the melt volume-flow rate (MVR) of thermoplastics," International Organization for Standardization, Geneva, Switzerland.

Lee, P., Chang, E., Yu, S., Lee, S. W., Kim, I. W., Park, S., and Chung, H. (2013). "Modification and characteristics of biodegradable polymer suitable for selective laser sintering," *Int. J. Precis. Eng. Man.*, 14(6) 1079-1086. DOI: 10.1007/s12541-013-0145-4

Marubayashi, H., Asai, S., and Sumita, M. (2012). "Complex crystal formation of poly(l -lactide) with solvent molecules," *Macromolecules* 45(3), 1384-1397. DOI: 10.1021/ma202324g

Mazzanti, V., and Mollica, F. (2017). "In-process measurements of flow characteristics of wood plastic composites," *J. Polym. Environ.* 25(4), 1044-1050. DOI: 10.1007/s10924-016-0876-2

Mazzanti, V., Mollica, F., and El Kissi, N. (2016). "Rheological and mechanical characterization of polypropylene-based wood plastic composites," *Polym. Composite.* 37(12), 3460-3473. DOI: 10.1002/pc.23546

Nakano, T., and Ishimoto, T. (2015). "Powder-based additive manufacturing for development of tailor-made implants for orthopedic applications," *KONA Powder Part. J.* (32), 75-84. DOI: 10.14356/kona.2015015

Poomathi, N., Singh, S., Prakash, C., Patil, R.V., Perumal, P. T., and Barathi, V. A. (2019). "Bioprinting in ophthalmology: Current advances and future pathways," *Rapid Prototyping J.* 25(3), 496-514. DOI: 10.1108/RPJ-06-2018-0144

Rezgui, F., Swistek, M., Hiver, J. M., G'Sell, C., and Sadoun, T. (2005). "Deformation and damage upon stretching of degradable polymers (PLA and PCL)," *Polymer* 46(18), 7370-7385. DOI: 10.1016/j.polymer.2005.03.116

Roberts, C. E ., Bourell, D., Watt, T., and Cohen, J. (2016). "A novel processing approach for additive manufacturing of commercial aluminum alloys," *Physics Procedia* 83, 909-917. DOI: 10.1016/j.phpro.2016.08.095

Rokkonen, T., Peltola, H., and Sandquist, D. (2019). "Foamability and viscosity behavior of extrusion foamed PLA-pulp fiber biocomposites," *J. Appl. Polym. Sci.* 136(41), 48202. DOI: 10.1002/app.48202

Schmid, M., Amado, A., and Wegener, K. (2014). "Materials perspective of polymers for additive manufacturing with selective laser sintering," *J. Mater. Res.* 29(17), 1824-1832. DOI: 10.1557/jmr.2014.138

Schmidt, M., Pohle, D., and Rechtenwald, T. (2007). "Selective laser sintering of PEEK," *CIRP Annals* 56(1), 205-208. DOI: 10.1016/j.cirp.2007.05.097

Shuai, C., Mao, Z., Han, Z., and Peng, S. (2014). "Preparation of complex porous scaffolds *via* selective laser sintering of poly(vinyl alcohol)/calcium silicate," *J. Bioact. Compat. Pol.* 29(2), 110-120. DOI: 10.1177/0883911514522570

Song, Y., Zhang, J., Zhang, X., and Tan, T. (2015). "The correlation between cellulose allomorphs (I and II) and conversion after removal of hemicellulose and lignin of lignocellulose," *Bioresource Technol.* 193, 164-170. DOI: 10.1016/j.biortech.2015.06.084

Speranza, V., De Meo, A., and Pantani, R. (2014). "Thermal and hydrolytic degradation kinetics of PLA in the molten state," *Polym. Degrad. Stabil.* 100(1), 37-41. DOI: 10.1016/j.polymdegradstab.2013.12.031

Tábi, T., Hajba, S., and Kovács, J. G. (2016). "Effect of crystalline forms (α' and α) of poly(lactic acid) on its mechanical, thermo-mechanical, heat deflection temperature and creep properties," *Eur. Polym. J.* 82, 232-243. DOI: 10.1016/j.eurpolymj.2016.07.024

Tábi, T., Wacha, A. F., and Hajba, S. (2018). "Effect of D-lactide content of annealed poly(lactic acid) on its thermal, mechanical, heat deflection temperature, and creep properties," *J. Appl. Polym. Sci.* 136(8), 47103. DOI: 10.1002/app.47103

Tan, K. H., Chua, C. K., Leong, K. F., Cheah, C. M., Cheang, P., Abu Bakar, M. S., and Cha, S. W. (2003). "Scaffold development using selective laser sintering of polyetheretherketone–hydroxyapatite biocomposite blends," *Biomaterials* 24(18), 3115-3123. DOI: 10.1016/S0142-9612(03)00131-5

Tan, K. H., Chua, C. K., Leong, K. F., Cheah, C. M., Gui, W. S., Tan, W. S., and Wiria, F. E. (2005). "Selective laser sintering of biocompatible polymers for applications in tissue engineering," *Bio-Med. Mater. Eng.* 15(1-2), 113-124.

Thittikorn, P., Pakorn, O., and Pisut, K. (2007). "Preparing biodegradable PLA for powder-based rapid prototyping," in: *The 8th Asia Pacific Industrial Engineering & Management System*, Taiwan.

Williams, J. M., Adewunmi, A., Schek, R. M., Flanagan, C. L., Krebsbach, P. H., Feinberg, S. E., Hollister, S. J., and Das, S. (2005). "Bone tissue engineering using polycaprolactone scaffolds fabricated *via* selective laser sintering," *Biomaterials* 26(23), 4817-4827. DOI: 10.1016/j.biomaterials.2004.11.057

Yang, S., Madbouly, S. A., Schrader, J. A., Srinivasan, G., Grewell, D., McCabe, K. G., Kessler, M. R., and Graves, W. R. (2015). "Characterization and biodegradation

behavior of bio-based poly(lactic acid) and soy protein blends for sustainable horticultural applications," *Green Chem.* 17(1), 380-393. DOI: 10.1039/c4gc01482k

Yu, Y., Guo, Y., Jiang, T., Li, J., Jiang, K., and Zhang, H. (2017). "Study on the ingredient proportions and after-treatment of laser sintering walnut shell composites," *Materials* 10(12), 1381-1393. DOI: 10.3390/ma10121381

Zhang, J., Tashiro, K., Tsuji, H., and Domb, A. J. (2008). "Disorder-to-order phase transition and multiple melting behavior of poly(l-lactide) investigated by simultaneous measurements of WAXD and DSC," *Macromolecules* 41(4), 1352-1357. DOI: 10.1021/ma0706071

Article submitted: April 9, 2020; Peer review completed: May 31, 2020; Revised version received: June 7, 2020; Accepted: June 8, 2020; Published: June 15, 2020.
DOI: 10.15376/biores.15.3.5886-5898